14th International Conference on Structural Safety and Reliability - ICOSSAR'25
1-6 June, 2025 - Los Angeles California, USA
R. Ghanem, E. Johnson, S. Masri and A. Olivier (Eds)

EFFECTS OF UNCERTAINTIES IN THE PARTICLE DISTRIBUTION OF RUBBER-SOIL MIXTURE ON THE PERFORMANCE OF SHALLOW FOUNDATIONS

F. MAKSIMOV[1], A. CONTENTO[2], B. BRISEGHELLA[2], P. CACCIOLA[2]

[1] School of Architecture, Technology and Engineering, University of Brighton
Cockcroft Building, Lewes Road, BN2 4GJ, Brighton, UK
F.Maksimov@brighton.ac.uk

[2] College of Civil Engineering, Fuzhou University
No.2 Xueyuan Rd., Minhou, Fuzhou, Fujian 350116, China
alessandro@fzu.edu.cn, bruno@fzu.edu.cn, p.cacciola@fzu.edu.cn

Key words: Geotechnical Seismic Isolation, Granular Materials, DEM, Soil Modeling.
Abstract. Modeling granular materials is essential for understanding their complex mechanical behaviors, particularly in soil-structure interaction (SSI), where factors like particle size, material properties, and boundary conditions influence structural response. Accurate SSI modeling is critical for geotechnical engineering applications, yet uncertainties in soil properties can significantly affect load distribution, deformation, and structural response. This study employs the open-source Discrete Element Method (DEM) software YADE (Yet Another Dynamic Engine) to analyze SSI dynamics, incorporating particle shape variability, contact models, and coupling with other numerical methods.

A key challenge in DEM simulations is the inherent uncertainty in particle packing, arising from random placement, particle size distribution deviations, and densification methods. To assess these uncertainties, a Monte Carlo approach is proposed to evaluate how variability in granulometric properties affects SSI parameters under different soil condition, namely: sand and rubber-soil mixtures—a material widely used in geotechnical seismic isolation (GSI) due to its unique deformable-granular behavior. The study investigates the impact of random particle distributions on critical SSI parameters, including lateral and rotational stiffness of shallow foundations, providing insights into uncertainty propagation and improving predictive accuracy for engineering design.

1 INTRODUCTION

Geotechnical Seismic Isolation (GSI) has gained increasing attention as an innovative strategy to protect structures from seismic hazards by modifying the soil-foundation interface rather than the superstructure itself [1]. Unlike conventional base isolation systems, which rely on engineered bearings or dampers integrated into the structure, GSI employs strategically designed soil layers to alter the dynamic response of the system. This approach offers several advantages, including lower costs, easier implementation in new and existing structures, and reduced maintenance requirements. Three primary mechanisms contribute to GSI performance: (1) frequency shift through low-stiffness layers [2,3], (2) energy dissipation via particle rearrangement and friction [4], and (3) controlled sliding at the soil-foundation interface [5].

The effectiveness of GSI systems depends critically on the mechanical behavior of the engineered soils used, which often consist of granular materials such as rubber-soil mixtures,

gravel, or geosynthetics [6–9]. A key challenge in GSI design lies in accurately characterizing the nonlinear and highly variable behavior of these granular materials under dynamic loading. Among the different materials investigated for GSI, rubber-soil mixtures have shown particular promise due to their ability to combine high damping with moderate stiffness, making them suitable for seismic isolation applications [9]. However, their mechanical response is inherently stochastic, influenced by factors such as particle size distribution, packing density, and interparticle friction.

Most existing studies on GSI are based on continuum-based numerical methods, and rely on equivalent linear methods [10] or nonlinear finite element (FE) models [11]. While these approaches provide valuable insights, they may overlook the discrete nature of granular materials, leading to potential inaccuracies in predicting soil-structure interaction (SSI) effects. Recent efforts have sought to refine SSI modeling through empirical calibrations of nonlinear springs [12,13] and advanced hysteresis models [14]. However, a fundamental gap remains in understanding how microscale particle-scale variability influences macroscale GSI performance.

To address this challenge, the present study utilizes the Discrete Element Method (DEM) within the YADE open-source framework [15] to explicitly model the behavior of rubber-soil mixtures, capturing the discontinuous and heterogeneous nature of granular materials. YADE (Yet Another Dynamic Engine) allows for precise control over particle geometry, contact laws, and boundary conditions, making it especially suitable for simulating the complex dynamics involved in soil-structure interaction (SSI). In this work, particle assemblies are generated through stochastic processes governed by a prescribed granulometric distribution, resulting in spatially randomized, non-overlapping configurations that reflect the inherent uncertainties in real-world materials. These initial packings are then subjected to gravity deposition and/or isotropic compression to achieve representative initial states. A Monte Carlo analysis is performed across multiple realizations of these randomized particle configurations to quantify how variability in particle size distribution and packing structure influences critical SSI parameters, particularly lateral and rotational stiffness of shallow foundations. This probabilistic approach provides insights into how microstructural uncertainties propagate into macroscale structural responses, thereby enhancing the predictive reliability of GSI systems.

2 FUNDAMENTALS OF SSI THROUGH LUMPED PARAMETER MODELS

In the context of modeling nonlinear soil-structure interaction (SSI), the lumped mass model provides a computationally efficient yet sufficiently accurate framework for capturing the essential dynamics of coupled soil and structural behavior. This modeling approach simplifies the system into discrete masses, while retaining key nonlinear and hysteretic features of the soil response. As described in [14], the structural system is typically idealized as a three-degree-of-freedom (3-DOF) model, where the superstructure is assumed to exhibit linear elastic behavior, and the foundation interacts with the surrounding soil through nonlinear, hysteretic springs.

The lumped mass model comprises concentrated masses representing the superstructure (denoted as m) and the foundation (m_F), interconnected via linear stiffness and damping components (k and c, respectively), as illustrated schematically in Fig. 1. The interaction between the foundation and the supporting soil is represented by two nonlinear hysteretic elements, $f_{u_F}(u_F,\dot{u}_F)$ and $f_\theta(\theta,\dot{\theta})$, associated with the translational (u_F) and rotational (θ)

degrees of freedom of the foundation, respectively. These hysteretic elements often follow hysteretic rules such as the Bouc-Wen [16] or Preisach [14] models, which can effectively simulate the energy dissipation and stiffness degradation observed in cyclic loading conditions. Under suitable assumptions, as in [14], they can be expressed in terms of equivalent damping and stiffness, c_{u_F} and k_{u_F} for $f_{u_F}(u_F,\dot{u}_F)$, and c_θ and k_θ for $f_\theta(\theta,\dot{\theta})$.

This modeling approach captures key SSI phenomena such as foundation rocking, radiation damping, and soil nonlinearity, all of which are critical under seismic loading. While simplified, the lumped mass model has been validated through comparisons with finite element simulations and centrifuge tests [13, 14], confirming its ability to reproduce important features of SSI systems under dynamic excitation [14].

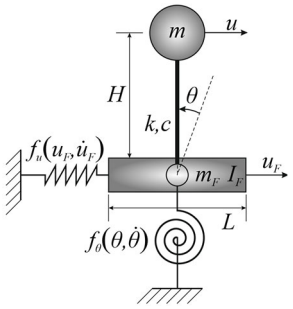

Figure 1: Lumped mass model

3 FUNDAMENTALS OF DEM FOR GEOTECHNICAL STUDY

Cundall and Strack [17] originally developed the Distinct Element Method (DEM), also known as the Discrete Element Method, for applications in soil mechanics, aiming to simulate the behavior of granular assemblies. In DEM, a granular medium is represented as a collection of discrete particles that interact at contact points through spring-dashpot systems. A major advantage of DEM lies in its capability to capture the material microstructure and explicitly model heterogeneity and dilative behavior. The method tracks the motion of each individual particle by solving their equations of motion at every time step, which must be sufficiently small to ensure numerical stability and accuracy.

For each particle i, characterized by radius r_i, mass m_i, and moment of inertia I_i, DEM explicitly integrates the following equations (Eqs. 1a and 1b):

$$m_i \cdot \ddot{\boldsymbol{x}}_i(t) = \widehat{\boldsymbol{F}}_i(t), \tag{1a}$$

$$\boldsymbol{I}_i \cdot \dot{\boldsymbol{\omega}}_i(t) = \widehat{\boldsymbol{M}}_i(t), \tag{1b}$$

in which $\ddot{x}_i$ is the acceleration of the center of mass of the particle, $\dot{\omega}_i$ is time-derivative of the particle's angular velocity of the center of mass of the particle, $\widehat{\boldsymbol{M}}_i$ is the resultant moment, and the contact force $\widehat{\boldsymbol{F}}_\mathrm{i}$ is the resultant force that includes the external load, all the contact forces with other particles, and the external damping force. For each contact ij between two spheres overlapping by δ_n, the contact forces in DEM can be evaluated using various formulations. Among the most widely adopted are the Cundall-Strack linear elastic model, the Hertz-Mindlin no-slip model, and the Mindlin-Deresiewicz partial-slip model. The equations of motion for each particle are integrated in time via an explicit time integration scheme (e.g., the leap-frog

algorithm). To ensure numerical stability, the timestep Δt must be sufficiently small to resolve the fastest contact-vibration, i.e., it must satisfy a Courant-type condition (Eq. 2) for the stiffest spring–mass element [18]:

$$\Delta t_{min} < \beta \cdot \sqrt{\frac{m_{min}}{k_{max}}} \approx \beta \cdot R_{min} \cdot \sqrt{\frac{\rho}{E}} \tag{2}$$

Here, m_{min} and k_{max} denote the smallest particle mass and maximum contact stiffness, respectively; R_{min} is the smallest particle radius, ρ is the particle density, E is Young's modulus, and β is a safety factor. The main disadvantage of the DEM is its substantial computational cost, primarily due to the need for contact detection and the calculation of contact forces and torques at each time step. This challenge becomes particularly pronounced in the modelling of real-scaled soil-structure interaction problems, which often involve hundreds of thousands of time steps to capture the full dynamic response. As a result, achieving feasible simulation times for large-scale problems remains an ongoing concern.

To address this issue, high-g scaling and centrifuge similarity laws offer an effective solution by reducing model domain size and simulation duration. Ting and Corkum [19] developed a small-scale DEM model using centrifuge-based scaling to minimize the number of particles while preserving the stress-strain equivalence with the full-scale prototype. Their simulations demonstrated that DEM, when combined with these scaling techniques, accurately reproduces soil–structure system responses from initial loading through to failure.

4 PSEUDO-CENTRIFUGE TEST WITH DEM

The numerical model inputs—including geometry, material properties, and boundary conditions—were directly derived from the centrifuge experiments conducted by Tsang et al. [20], who investigated geosynthetic-reinforced rubber-soil mixture (RSM) systems with varying rubber content, using tests with pure gravel as a reference baseline. A detailed description of the model configuration is provided below.

4.1 Geometry

To investigate soil-structure interaction, a centrifuge-scaled numerical model was developed to simulate a rectangular footing (18 m × 12 m in plan) founded on two different soil conditions: (i) pure gravel and (ii) RSM layer underlain by gravel, as described in [20]. A shallow embedment depth of 1 m was assumed, and the footing was modeled as a rigid body. The soil domain measured 35.5 m × 26 m × 7.5 m (depth), while the RSM layer extended over an area of 22 m × 16 m with a thickness of 3 m. Fig. 2 presents the reduced-scale model obtained following the centrifuge scale approach. These simulations were performed under 50g gravitation (scale factor = 50g).

4.2 Gravel and soil-rubber mixture discrete model characterization

In this study, two foundation materials were modeled to evaluate their influence on soil-structure interaction:

1. *Pure gravel*: A 3D assembly of spherical particles with radii sampled from the gravel's granulometric curve, interpreted as a cumulative distribution function (CDF). The

particle sizes ranged from 6.35 mm to 9.53 mm, with a median diameter D_{50} = 7.3 mm.

2. *Rubber- Soil Mixture* (30 wt.%): The same gravel assembly was modified by introducing rubber particles constituting 30% of the total weight. The rubber inclusions were also modelled as spheres, with a prescribed median diameter D_{50} = 3.1 mm.

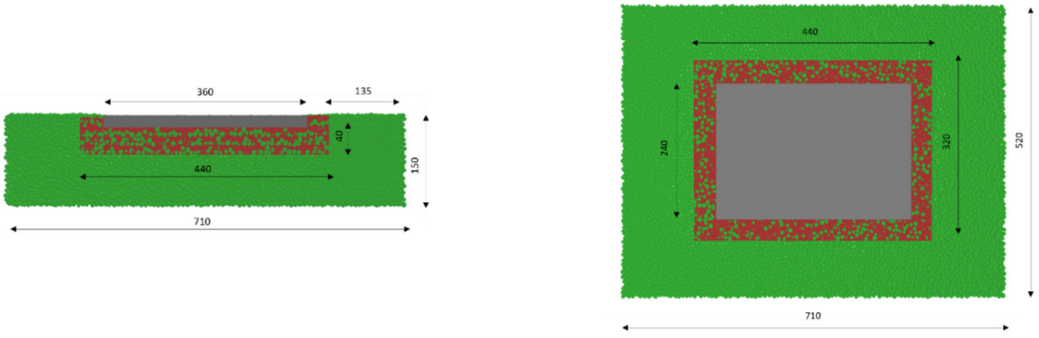

(a) (b)

Figure 2: Reduced-scale model (measures in mm): (a) Lateral view; (b) Top view.

5 MODELLING METHODOLOGY

The DEM simulations based on centrifuge principles were performed using the open-source code YADE [17]. However, the proposed methodology is sufficiently general to be implemented within any comparable DEM framework. To validate the DEM simulations and investigate the rocking and lateral translational response of shallow foundations within the GSI-RSM system, a three-stage approach was adopted, namely: 1) Calibration of the contact law parameters; 2) Preparation of the DEM model (DEM model preparation); 3) Execution of simulations and post-processing of the results (Analyses).

5.1 Calibration of the contact law parameters

Both the normal and tangential contact forces were computed using the Hertz-Mindlin no-slip formulation [18]. Briefly, the Hertz-Mindlin no-slip contact law is fully defined by four parameters: the Young's modulus E_i of the particles, the Poisson's ratio υ, the inter-particle friction coefficient μ and the particle radius r_i. The radius, r_i, of each i-th particle, was sampled according to the particle size distribution of the foundation material.

To account for the compressive volumetric behavior of rubber, the rubber particles were modelled as deformable spheres. Deformation is modelled by expanding the particle radius based on the extent of overlap, such that the total volume of the material remains constant [21].

The calibration of the DEM contact model parameters (see Table 1) was performed through a series of 3D cyclic triaxial test simulations using a periodic cubic cell.

Table 1: Model Parameters

Parameter	Gravel	Rubber
Density, ρ [kg/m³]	2650	1200
Poisson's ratio, ν	0.12	0.48
Young modulus *E, Pa*	1×10^9	$1\times10^9/350$
Inter-particle friction coefficient, μ	0.7 (35)	0.83 (40)
Number of particles (1 pack)	265000	470000
Timestep [s]	2.11×10^{-6}	1.57×10^{-6}

The simulation results were compared against experimental shear modulus reduction and damping curves reported by Senetakis et al. [22] and referenced in Tsang and Pitilakis [10]. The optimal contact model parameters, listed in Table 1, correspond to the best fit between the simulated and experimental shear modulus degradation and damping behavior as functions of shear strain amplitude.

5.2 DEM model preparation

A 3D prismatic domain was defined, with all faces modeled as rigid, frictionless walls to enforce a rigid-wall boundary condition. The sample preparation involved three main steps: (a) random generation of non-contacting particles in the prismatic domain; (b) numerical consolidation of the assembly; and (c) generation of the shallow foundation.

Following this approach, 300 independent packs were generated for each SSI model (i.e., gravel-only and RSM configurations). These simulations were executed on a high-performance computing (HPC) cluster, with each assembly generation parallelized across multiple compute nodes. Within each pack, the particle distribution was determined using a Monte Carlo approach based on four independent random variables: the three spatial coordinates (uniformly distributed) and the particle radius, sampled according to the specified particle size distribution

Random sample generation: This first step involves generating numerical specimens that capture the variability of soil microstructure—namely grain size, distribution, and spatial arrangement—which governs inherent anisotropy and fabric evolution under load. The random sample generation is performed according to the following procedure:

- A placement volume (the "placement zone") is defined, sufficiently large to accommodate all particles without initial overlaps;
- This volume is subdivided into equal-sized cubic cells;
- In each cell, a single particle is placed at a random location: For the gravel-only case, particle sizes are sampled from the soil particle size distribution. For the gravel-rubber mixture, each particle is randomly selected from one of two pre-generated clouds—gravel or rubber—and then placed accordingly;
- Particle radii are sampled via inverse transform sampling from the prescribed particle size distributions. Placement within each cubic cell is random, with careful checking to avoid initial overlaps. This approach ensures that the resulting particle assemblies are in a gas-like, stress-free state prior to the application of any loading or consolidation.

Numerical consolidation: In this step, the assembly is allowed to settle under an accelerated gravity field (50 g) until it reaches static equilibrium.

It has to be emphasized that packing density (porosity) plays an essential role in defining the overall (macroscopic) stress-strain behavior of the material. Numerical specimens with specific relative densities are obtained by assigning a fictitious interparticle friction angle during the deposition phase. When a friction angle of 1° is used, the resulting mean void ratio is approximately 0.43, corresponding to a dense packing condition. This matches the relative density (approximately 70%) of the sand specimens used in the centrifuge experiments conducted by Tsang (2020) [20].

Foundation generation: Soil spheres are first generated uniformly throughout the entire computational domain. Simultaneously, RSM (rubber) spheres are generated in a separate sub-volume corresponding to the RSM layer. Once both assemblies reach static equilibrium, all soil

particles with centers located within the RSM zone are removed. The thicker low-modulus RSM layer is then inserted into the vacated volume (Fig. 3). Subsequently, the footing slab is positioned by removing any overlapping RSM particles within its footprint and placing the foundation and structural load elements in the cleared space. Finally, the complete assembly—including soil, RSM layer, slab, and superstructure—is allowed to reach mechanical equilibrium under self-weight.

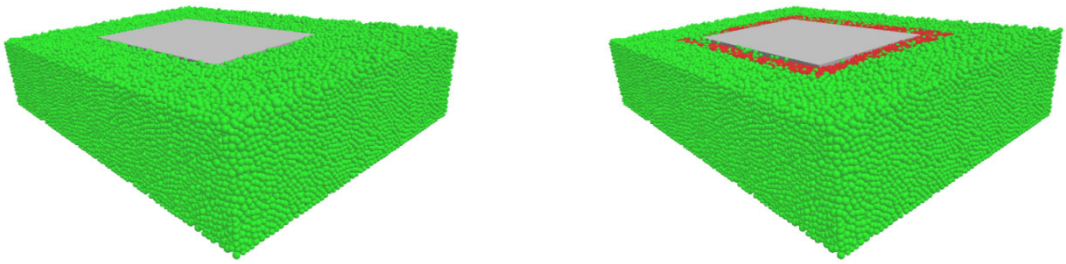

(a) (b)

Figure 2: Samples of two randomly generated SSI models: (a) Gravel-only; (b) RSM.

5.3 Analyses

Kinematic control is employed to perform DEM simulations under both monotonic and cyclic loading conditions, where the shallow foundation is subjected to translational and rotational displacements prescribed velocities. A constant lateral displacement rate of $\dot{u}_F = 0.05$ m/s and a constant angular velocity of $\dot{\theta} = 0.01$ rad/s are imposed at the base of the foundation.

In the translational stage, the footing translates laterally until a target displacement of $u_F = 0.03 \cdot L$ is reached, where L is the foundation length. Similarly, in the rotational stage, the footing rotates at a constant angular velocity until a total rotation angle of $\theta = 3°$ is attained.

Monotonic tests are conducted under the prescribed kinematic conditions to evaluate the lateral and rotational stiffness of the foundation.

Cyclic tests are performed using sinusoidal excitation at varying frequencies, adjusted to maintain a constant velocity while varying the amplitude. Each test batch consists of 320 samples, with translational amplitudes ranging from $0.001 \cdot L$ to $0.008 \cdot L$ and rotational amplitudes ranging from 0.001 rad to 0.02 rad. By analyzing the resulting force-displacement and moment-rotation hysteresis loops at each amplitude, the equivalent viscous damping coefficients for both translation and rotation are extracted.

6 NUMERICAL RESULTS

This section presents the results of both monotonic and cyclic tests. Specifically, Figs. 4 and 5 show the variations of the lateral stiffness (k_{u_F}, Fig. 4) and rotational stiffness (k_θ, Fig. 5) as functions of increasing values of translational and rotational displacements for both the gravel-only and RSM configurations.

In these figures, the thin black curves represent the individual simulations outcomes, whereas the thicker dashed red lines indicate the mean values across all realizations. It is observed that both mean values and the associated variability largely decrease with increasing displacements, showing a tendency toward asymptotic stabilization, thereby reducing the influence of initial uncertainties in the SSI models.

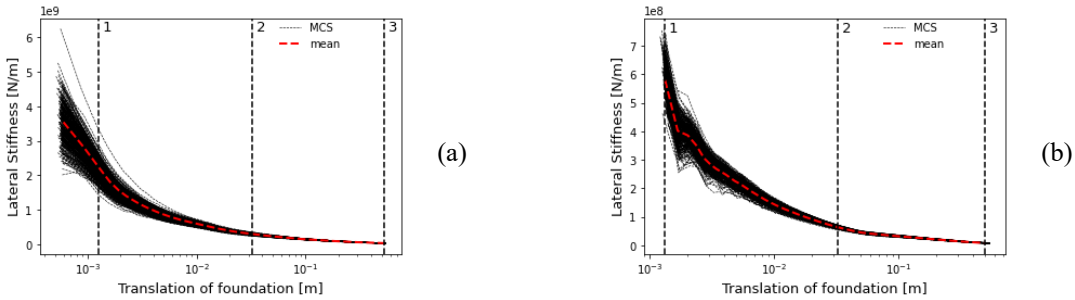

Figure 4: Lateral stiffness of the shallow foundation: (a) Gravel-only; (b) RSM.

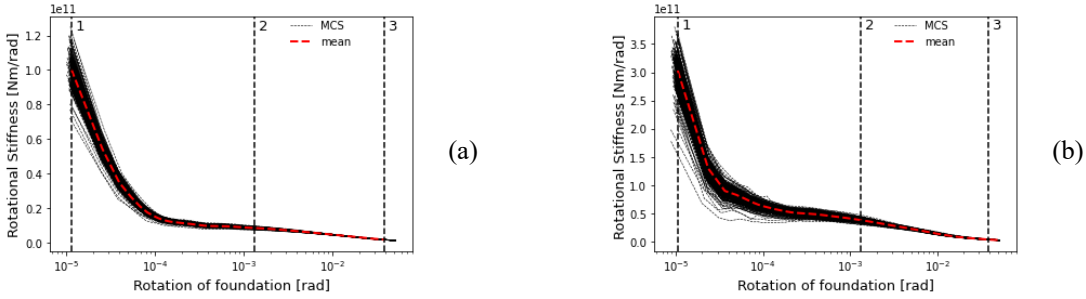

Figure 5: Rotational stiffness of the shallow foundation: (a) Gravel-only; (b) RSM.

Figs. 6 and 7 present the empirical distributions of the lateral and rotational stiffnesses, respectively, at selected displacement levels, which correspond to the values marked by vertical black dashed lines in Figs. 4 and 5. The corresponding statistical descriptors, namely the mean values and coefficients of variation (COV), are summarized in Table 2.

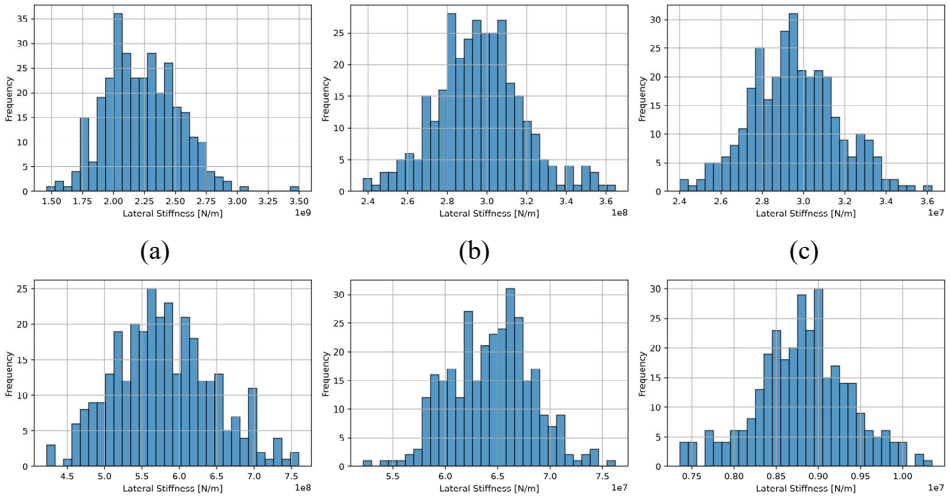

Figure 5: Distributions of the lateral stiffness of the shallow foundation for gravel-only ((a), (b), (c)) and RSM ((d), (e), (f)) at selected displacements: (a), (d) u_F = 0.0013 m; (b), (e) u_F = 0.032 m; (c), (f) u_F = 0.525 m.

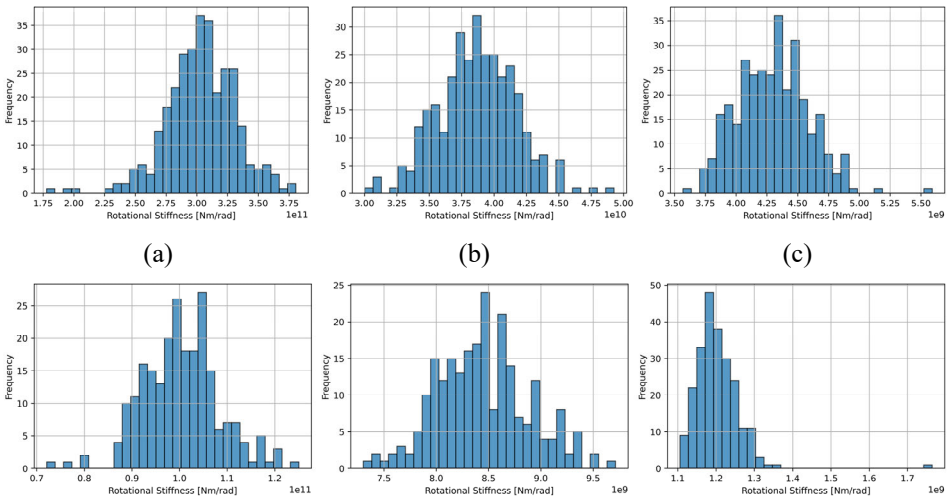

Figure 7: Distributions of the rotational stiffness of the shallow foundation for gravel-only ((a), (b), (c)) and RSM ((d), (e), (f)) at selected rotations: (a), (d) $\theta = 1.1\times10^{-5}$ rad; (b), (e) $\theta = 0.0013$ rad; (c), (f) $\theta = 0.0387$ rad.

Comparing the gravel-only and RSM cases, it is observed that the gravel-only configuration exhibits not only higher mean stiffness values, as expected, but also slightly greater variability.

Table 2: Statistics of the distributions of translational and rotational stiffnesses

	Gravel		**RSM**	
Lateral displacement [m]	k_{u_F} mean [N/m]	k_{u_F} COV	k_{u_F} mean [N/m]	k_{u_F} COV
0.13×10^{-2}	2.23×10^{9}	0.130	5.80×10^{8}	0.110
3.20×10^{-2}	2.96×10^{8}	0.074	6.40×10^{7}	0.061
5.25×10^{-1}	2.90×10^{7}	0.071	8.80×10^{6}	0.063
Rotation [rad]	k_θ mean [N·m/rad]	k_θ COV	k_θ mean [N·m/rad]	k_θ COV
0.11×10^{-4}	3.03×10^{11}	0.094	1.00×10^{11}	0.080
0.13×10^{-2}	3.87×10^{10}	0.077	8.45×10^{9}	0.052
3.87×10^{-2}	4.30×10^{9}	0.067	1.20×10^{9}	0.049

Figs. 8 and 9, analogous to Figs. 4 and 5, illustrate the variations of the damping with increasing displacements. Specifically, Figs. 8a and 8b depict the translational damping behavior for the gravel-only and RSM configurations, respectively, while Figs. 9a and 9b present the corresponding results for rotational damping.

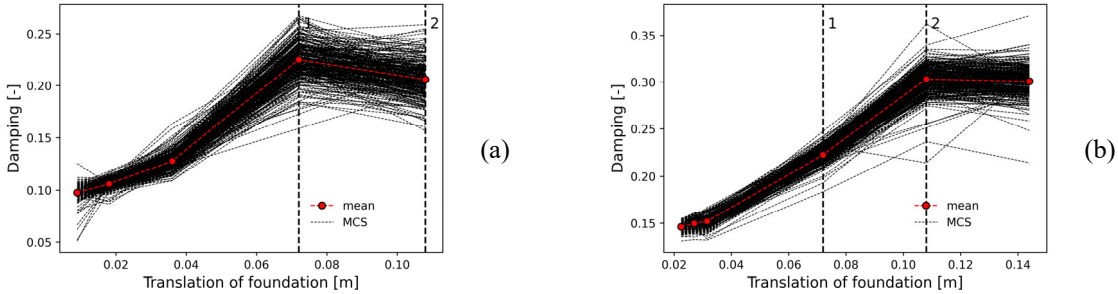

Figure 8: Translational damping of the shallow foundation: (a) Gravel-only; (b) RSM.

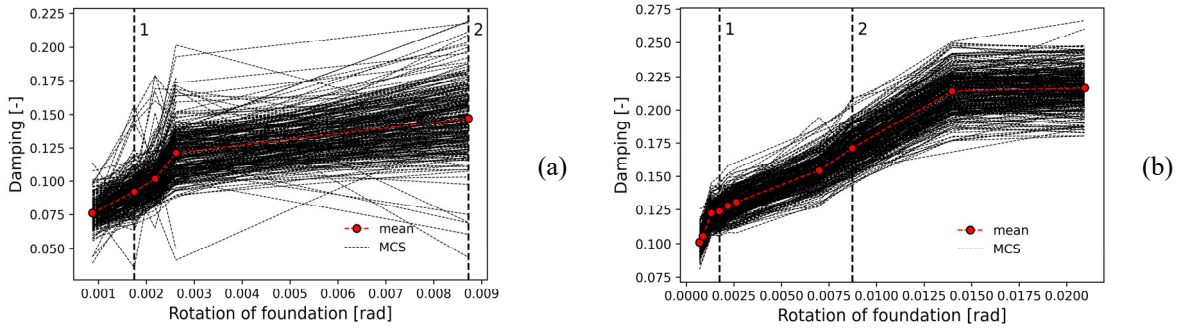

Figure 9: Rotational damping of the shallow foundation: (a) Gravel-only; (b) RSM.

Figs. 10 and 11 display the empirical distributions of the translational and rotational damping, respectively, at selected displacement levels indicated by the vertical black dashed lines in Figs. 8 and 9. The corresponding statistical measures are summarized in Table 3.

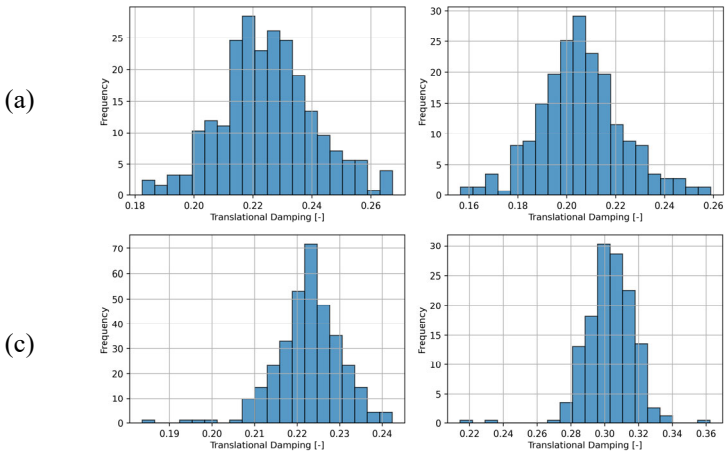

Figure 10: Distributions of the translational damping of the shallow foundation for gravel-only ((a), (b)) and RSM ((c), (d)) at selected displacements: (a), (c) $u_F = 0.0013$ m; (b), (d) $u_F = 0.032$ m.

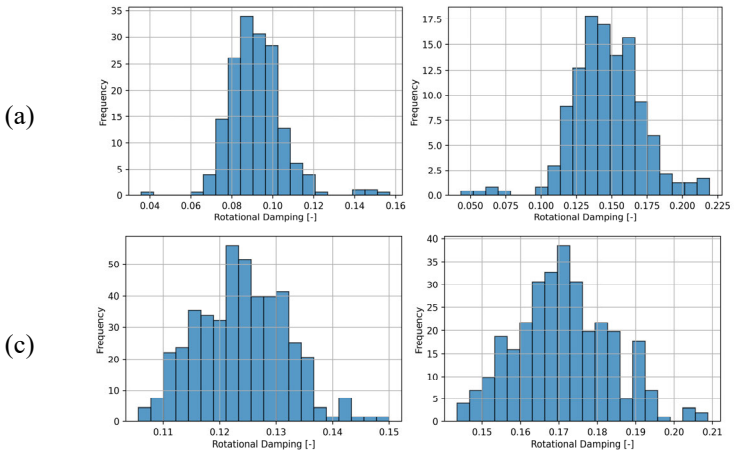

Figure 11: Distributions of the rotational damping of the shallow foundation for gravel-only ((a), (b)) and RSM ((c), (d)) at selected rotations: (a), (d) $\theta = 1.75 \times 10^{-3}$ rad; (b), (e) $\theta = 8.73 \times 10^{-3}$ rad.

Table 3: Statistics of the distributions of translational and rotational damping

	Gravel		**RSM**	
Lateral displacement [m]	c_{u_F} mean	c_{u_F} COV	c_{u_F} mean	c_{u_F} COV
0.072	0.224	0.070	0.220	0.034
0.108	0.205	0.083	0.303	0.046
Rotation [rad]	c_θ mean	c_θ COV	c_θ mean	c_θ COV
1.75 ×10−3 rad	0.092	0.147	0.123	0.064
8.73× 10−3 rad	0.147	0.169	0.170	0.072

For the damping, the mean values initially exhibit a rapid increase with displacement, followed by a slight decreasing trend for translational damping and a slight increasing trend for rotational damping in the gravel-only configuration (Figs. 8a and 9a, respectively). In contrast, the RSM configuration shows a stabilization toward nearly constant values for both translational and rotational damping (Figs. 8b and 9b). When comparing the two configurations, the RSM configuration results in higher mean damping values but lower variability.

In contrast to the behavior observed for stiffness, the variability in damping values increases with displacement. This behavior is likely due to the greater uncertainty introduced by the progressive widening of the hysteresis loops at higher deformation levels.

6 CONCLUSIONS

This study clarifies the influence of microscale variability in particle distribution on the macroscale behavior of shallow foundations, particularly when RSM are employed for GSI applications. Monte Carlo-based DEM simulations demonstrated that initial uncertainties in particle packing induce significant variability in both stiffness and damping parameters at small displacements. As displacements increase, the variability in stiffness progressively stabilizes, whereas the variability in damping exhibits an increasing trend, potentially amplifying uncertainties in the modeling of the structural response.

Comparisons between gravel-only and rubber-soil mixture configurations further confirmed that rubber inclusions effectively reduce stiffness while enhancing energy dissipation, offering potential advantages for seismic isolation applications.

REFERENCES

[1] Tsang, H.H. Seismic isolation by rubber–soil mixtures for developing countries. *Earthq. Eng. Struct. Dyn.* (2008) **37**(2):283-303.

[2] Aloisio, A., Contento, A., Xue, J., Fu, R., Fragiacomo, M., and Briseghella, B. Probabilistic formulation for the q-factor of piles with damping pre-hole. *Bull. Earthq. Eng.* (2023) **21**(8):3749–3775.

[3] Tsang, H.H. 2023. Analytical design models for geotechnical seismic isolation systems. *Bull. Earthq. Eng.* (2023) **21**(8):3881-3904.

[4] Hazarika, H., Kuribayashi, K., Kuroda, S., and Hu, Y. Performance evaluation of waste tires in protecting embankment against earthquake loading. *Bull. Earthq. Eng.* (2023) **21**(8):4019-4035.

[5] Banović, I., Radnić, J., Grgić, N., and Semren, K. Effectiveness of several low-cost geotechnical seismic isolation methods: a shake-table study. *Bull. Earthq. Eng.* (2023) **21**(8):3923–3947.

[6] Kalpakcı, V., Bonab, A.T., Özkan, M.Y., and Gülerce, Z. Experimental evaluation of geomembrane/geotextile interface as base isolating system. *Geosynth. Int.* (2018) **25**(1):1-11.
[7] Patil, S.J., Reddy, G.R., Shivshankar, R., Babu, R., Jayalekshmi, B.R., and Kumar, B. Seismic base isolation for structures using river sand. *Earthq. Struct.* (2016) **10**(4):829-847.
[8] Banović, I., Radnić, J., and Grgić, N. Foundation size effect on the efficiency of seismic base isolation using a layer of stone pebbles. *Earthq. Struct.* (2020) **19**(2):103-117.
[9] Forcellini, D. Fragility Assessment of Geotechnical Seismic Isolated (GSI) Configurations. *Energies* (2021) **14**(16):5088.
[10] Tsang, H.H. and Pitilakis, D. Mechanism of geotechnical seismic isolation system: Analytical modelling, *Soil Dyn. Earthq. Eng*. (2019) **122**:171-184.
[11] Tsang, H.H., Lo, S.H., Xu, X., and Sheikh, M.N. Seismic isolation for low-to-medium-rise buildings using granulated rubber-soil mixtures: numerical study. *Earthq. Eng. Struct. Dyn.* (2012) **41**:2009-2024.
[12] Gazetas, G., Anastasopoulos, I., Adamidis, O., and Kontoroupi, T. Nonlinear rocking stiffness of foundations. *Soil Dyn. Earthq. Eng.* (2013) **47**:83-91.
[13] Li, Z., Escoffier, S., and Kotronis, P. Study on the stiffness degradation and damping of pile foundations under dynamic loadings. *Eng. Struct.* (2020) **203**:109850.
[14] Cacciola, P. and Tombari, A. Steady state harmonic response of nonlinear soil-structure interaction problems through the Preisach formalism. *Soil Dyn. Earthq. Eng.* (2021) **44**:106669.
[15] Šmilauer, V., Angelidakis, V., Catalano, E., Caulk, R., Chareyre, B., Chèvremont, W., Dorofeenko, S., Duriez, J., Dyck, N., Eliáš, J., Er, B., Eulitz, A., Gladky, A., Guo, N., Jakob, C., Kneib, F., Kozicki, J., Marzougui, D., Maurin, R., Modenese, C., Pekmezi, G., Scholtès, L., Sibille, L., Stransky, J., Sweijen, T., Thoeni, K., and Yuan, C. Yade Documentation (3rd ed.). The Yade Project (2021). DOI: 10.5281/zenodo.5705394
[16] Aloisio, A., Alaggio, R., Köhler, J., and Fragiacomo M. Extension of Generalized Bouc-Wen Hysteresis Modeling of Wood Joints and Structural Systems. *J. Eng. Mech.* (2020) **146**(3): 04020001.
[17] Cundall, P.A. and Strack, O.D.L. A discrete numerical model for granular assemblies. *Géotechnique* (1979) **29**(1):47-65.
[18] Radjai, F. and Dubois, F. *Discrete-element modeling of granular materials*. Wiley-ISTE (2011).
[19] Ting, J.M. and Corkum, B.T. Computational laboratory for discrete element geomechanics. *J. Comput. Civ. Eng.* (1992) **6**(2):129–146.
[20] Tsang, H.H., Tran, D.P., Hung, W.Y., Pitilakis, K., and Gad, E.F. Performance of geotechnical seismic isolation system using rubber–soil mixtures in centrifuge testing. *Earthq. Eng. Struct. Dyn*. (2021) **50**(5):1271-1289.
[21] Haustein, M., Gladkyy, A., and Schwarze R. Discrete element modeling of deformable particles in YADE. *SoftwareX* (2017) **6**:118-123.
[22] Senetakis, K., Anastasiadis, A., and Pitilakis, K. Dynamic properties of dry sand/rubber (RSM) and gravel/rubber (GRM) mixtures in a wide range of shearing strain amplitudes. *Soil Dyn. Earthq. Eng.* (2012) **33**:38-53.